УДК 621. 373.826 **DOI:10.30837/rt.2025.3.222.20**

S.S. HERASYMOV, O.S. HNATENKO, Ph.D.

SILVER FILM AND DISTRIBUTED BRAGG REFLECTOR MICROCAVITY: MULTILAYERED LASER MODEL THRESHOLD ANALYSIS

Introduction

With the growing demand for miniaturized and integrated optical systems, traditional solid-state lasers are being increasingly replaced by microlasers. These compact devices offer superior monochromaticity, higher beam quality, lower noise, and seamless integration with micro- and nanoelectronics systems, unlocking new perspectives in technologies [1–3]. A significant category of microlasers includes the VCSEL (Vertical-Cavity Surface-Emitting Laser) and photonic crystal surface-emitting laser (PCSEL) [4]. VCSEL and PCSEL emit visible or infrared light perpendicularly to the surface of the fabricated wafer. They are commonly used in data communication and sensing applications and are becoming increasingly popular in light detection and ranging (LiDAR) applications due to their energy efficiency and high precision [5–7].

Rare-earth (RE) ions-activated micro- and nanomaterials have emerged as promising candidates for next-generation microlasers, offering advantages such as cost-effective fabrication, high environmental stability, and broad spectral coverage from ultraviolet to mid-infrared [8]. Their high photoluminescence quantum yield (PLQY) and low surface defect density enhance their optical performance. Recent advancements in RE ions-activated luminescent materials, coupled with the development of novel micro- and nanocavities for optical feedback, have significantly improved laser efficiency and stability [9–11]. These innovations have driven substantial progress in the field, paving the way for highly efficient, miniaturized laser sources with applications in optical communication, sensing, and integrated photonics [6, 10, 12]. The rare-earth doped yttrium aluminum garnet (YAG) crystal is one of most popular, and reliable lasing gain material in conventional solid-state bulk lasers. By doping YAG with different rare-earth elements, it enables laser emission over a broad wavelength range. For example, the Nd:YAG crystal, featuring a four-level laser system, offers an exceptionally low lasing threshold, making it ideal for on-chip applications, nonlinear optics, and biosensing [12]. It has been widely explored as a waveguide-based on-chip light source.

Layered microlasers are an emerging class of compact laser devices that use multiple stacked layers of optical and gain materials to enhance performance and tunability. By carefully designing these layers, researchers achieve improved photon confinement, lower lasing thresholds, and broader spectral control, making them highly efficient and versatile. Common structures include distributed Bragg reflectors (DBRs), dielectric-metal-dielectric (DMD) stacks, and heterostructures incorporating quantum wells or 2D materials. These microlasers are also promising for applications in on-chip photonics, optical communication, LiDAR, and biosensing, as they can be seamlessly integrated into micro- and nanoscale systems [13, 14]. Recent advancements, such as perovskite-based microlasers, rare-earth-doped structures, and graphene-enhanced designs, have further expanded their potential by enabling tunable, high-quality lasing across ultraviolet to infrared wavelengths. Their small size, low power consumption, and compatibility with silicon-based platforms position layered microlasers as key components in next-generation photonic and optoelectronic technologies [8].

In microlaser structures, silver is commonly employed due to its superior plasmonic properties, which enhance light confinement and amplification at the nanoscale. For instance, integrating silver nanorings with silica microcavities has been shown to achieve high-quality hybrid plasmonic modes, facilitating efficient lasing in compact designs [15]. The pure silver has the highest reflectivity of all noble metals, particularly in the visible and near-infrared regions [16]. Additionally, the use of atomically smooth epitaxial silver films in plasmonic nanocavities has demonstrated reduced optical losses, leading to improved performance in nanolaser applications [17]. The noble metal, including silver, cavities are widely investigated and have some drawbacks as sizable ohmic losses.

Alternative reflector could be dielectric DBR, consist of high and low refractive indices layers. Their high reflectivity helps reduce radiation losses, thereby lowering the lasing threshold. These structures are commonly fabricated using the reliable method of metal-organic chemical vapor deposition (CVD), which enables precise control of both layers' composition and thickness. DBRs offer a compact and flexible design, allowing for tailored reflectivity and wavelength properties to suit specific applications [13]. In general, modern microlaser designs use distributed Bragg reflectors and noble metal cavity components to improve their efficiency and overall performance.

Understanding the lasing threshold conditions is crucial in laser design and development. Since laser emission is influenced by multiple physical mechanisms, full modeling presents a complex theoretical challenge. By neglecting all non-electromagnetic effects and focusing on electromagnetic fields, we can simplify the analysis and use a source-free linear Maxwell's equations, along with boundary conditions at edges and the radiation condition at infinity. The key aspect is considering the presence of the active region. This method, known as the Lasing Eigenvalue Problem (LEP), is described in detail in [18, 19]. This approach allows examination of specific modes' threshold values of the gain index along with its emission frequencies. These two parameters are treated as ordered, mode-specific two-component eigenvalues, which include the wavelength and the threshold gain index. Over the past two decades, the LEP has been applied to various material and shape micro- and nanolaser models to analyze their threshold conditions [20–23]. Recently, we have used such approach to investigate the host gain materials and their thickness impact in the laser microcavity [24] and the noble metal-walled cavity microlaser configuration [25].

In this paper, we use the LEP approach to analyze the thresholds conditions for the modes of the active cavity, sandwiched between a finite-thickness silver film and substrate made of full dielectric DBR.

1-D lasing eigenvalue problem formulation and basic equations

Laser modes on the stationary emission threshold, in the LEP approach, can be considered as open cavity's natural modes with natural frequencies, which are real-valued. As is known from Poynting theorem, purely real natural frequencies are forbidden in passive open cavities, however, the presence of active regions permits such frequencies. Then, we seek these laser modes as solutions of the source-free, time-harmonic Maxwell equations defined over an infinite spatial domain, subject to appropriate boundary and radiation conditions.

Fig. 1 illustrates the one-dimensional microlaser configuration under consideration, comprising an active layer filled with gain material, a silver superstrate film, and a substrate DBR composed of alternating dielectric layer. The time dependence is presented as $e^{-i\omega t}$, where $\omega > 0$, positive cyclic frequency. Then, we assume that the gain material has a complex relative dielectric permittivity $\varepsilon_c = \varepsilon' + i\varepsilon''$ featuring a negative imaginary part, which is responsible for gain effect in this consideration. The silver film dielectric permittivity is denoted as $\varepsilon_f(\lambda)$ while all materials are considered nonmagnetic. In laser science, the gain material is traditionally characterize1d020. equivalently by its refractive index $\nu = \sqrt{\varepsilon_c} = \alpha_c - i\gamma$. Here, the cavity is supposed uniformly active, so that $\alpha_c = \mathrm{Re}\,\nu > 0$ is the known chosen material refractive index, and $\gamma = -\mathrm{Im}\,\nu > 0$, is unknown threshold gain index value. The silver film refractive index $\alpha_f(\lambda) = \sqrt{\varepsilon_f}$ has positive imaginary part responsible for the ohmic losses. We obtain these values from the experimental data presented in [26], using the Akima spline interpolation method for smooth estimation. It is well established that the bulk refractive index can be applied when the size of the metal particles or the film thickness, in our case, exceeds the electron path without collision in the metal, which is approximately 3□nm. For modelling, we assume a frequency-independent gain index for wider versatility.

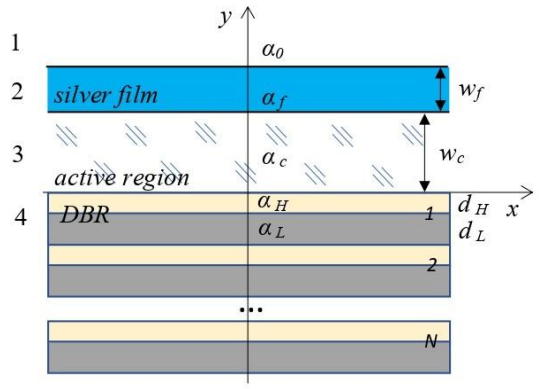

Fig. 1. Schematic laser model composed of a fully active region, covered by a finite-thickness silver film and supported by a finite distributed Bragg reflector (DBR)

The field function off the layer's boundaries must satisfy the Helmholtz equation as presented in (1). There, as *E*-field does not vary along x and z-axes, we have to look for a scalar function *E*(*y*), which represents the E_z field component.

$$\left(\Delta + k_D^2\right) E(y) = 0, \quad y_D < y < y_{D+1}, \tag{1}$$

where $D = 1, \ldots Q + 1$ is the domain number counted from the air halfspace above the silver film and y_D is the boundary coordinate, so that $Q = 4+2N$ for the cavity with DBR, N is the number of layer pairs. Besides, $k_1 = k = \omega / c$ is the free space wavenumber, $k_2 = k_f = k\alpha_f$, $k_3 = k_c = k\nu$ in the cavities. For DBR, the wavenumber values k_n, where $n \geq 4$, alternate between the higher and lower reflective index layers. In this paper, the adjacent to the cavity layer of DBR has higher refractive index, therefore, $k_{4+2n} = k_H = k\alpha_H$, $k_{5+2n} = k_L = k\alpha_L$, $n = 1,...,N-1$, and the DBR opens to the free halfspace, i.e. $k_{2N+4} = k$.

The electromagnetic field tangential components must remain continuous across the interfaces of material.

$$E^{(\mathrm{D})}(y) = E^{(\mathrm{D}+1)}(y)\Big|_{y=y_D}, \qquad \frac{\partial}{\partial y}\left(\frac{1}{\mu_D}E^{(\mathrm{D})}(y) - \frac{1}{\mu_{D+1}}E^{(\mathrm{D}+1)}(y)\right)\Bigg|_{y=y_D} = 0 \quad , \tag{2}$$

where $y_1 = w_c + w_f$, $y_2 = w_c$, $y_3 = 0$, and additional boundaries, y_n with $n = 4, \ldots, 3+2N$, correspond to the interfaces between the DBR layers, and $y_{4+2N} = -(w_L + w_H)N$. Additionally, the field function must exhibit outgoing wave behaviour in accordance with the radiation condition, as follows

$$E(y) = C\, e^{ik|y|}, \quad y \to \pm\infty \tag{3}$$

To analyse the threshold conditions using the LEP, we seek the eigenvalues of equations (1) – (3) as pairs of real numbers (λ_m, γ_m): the first representing the emission wavelengths, and the second corresponding to the gain index threshold values of laser modes.

By substituting the relevant electric field expressions into the boundary conditions at the interfaces and performing some algebraic manipulations, the LEP simplifies to the following transcendental equation:

$$\Phi(k,\gamma) = e^{-i2k(\alpha_c - i\gamma)w_c} - \frac{R_{DBR}\left(e^{i2k\alpha_M w_f} R_{12} - R_{32}\right)}{e^{i2k\alpha_M w_f} R_{12}R_{32} - 1} = 0\,, \tag{4}$$

where

$$R_{jp} = \left(\alpha_j - \alpha_p\right)\left(\alpha_j + \alpha_p\right)^{-1},\ j \neq p\ , \tag{5}$$

are the reflection coefficients from the interfaces between the corresponding domains.

For deriving the reflection coefficient of DBR, R_{DBR}, we apply the Transfer Matrix Method (TMM). As detailed in [19], the corresponding transfer matrix, $\mathbf{M}$, for L-layer dielectric structure can be obtained as a product of transmittance matrices between the neighbouring layers, $\mathbf{T}(\alpha_{i+1}/\alpha_i)$, and propagation matrices in each layer $\mathbf{P}(\alpha_i k d_i)$, namely

$$\mathbf{M} = \begin{pmatrix} m_{11} & m_{12} \\ m_{21} & m_{22} \end{pmatrix} = \mathbf{T}\left(\frac{\alpha_1}{\alpha_c}\right) \cdot \prod_{i=1}^{L-1} \mathbf{P}(\alpha_i k d_i)\mathbf{T}\left(\frac{\alpha_{i+1}}{\alpha_i}\right) \cdot \mathbf{P}(\alpha_L k d_L)\mathbf{T}\left(\frac{\alpha_{air}}{\alpha_L}\right), \tag{6}$$

where $\mathbf{T}(z) = \frac{1}{2}\begin{pmatrix} 1+z & 1-z \\ 1-z & 1+z \end{pmatrix}$, $\mathbf{P}(x) = \begin{pmatrix} e^{-ix} & 0 \\ 0 & e^{ix} \end{pmatrix}$

Afterward, the reflection and transmission coefficients of DBR as follows

$$R_{DBR} = \frac{m_{21}}{m_{11}},\ T_{DBR} = \frac{1}{m_{11}} \tag{7}$$

Therefore, we seek the LEP eigenvalues, which correspond to the roots of the equation (4). To determine their precise locations, a gradient-based iterative search algorithm is used.

Active microcavity featuring silver film and distributed Bragg reflector

As mentioned previously, we studied the silver-walled microcavity laser structure in [25], it consisted of a top silver film, a gain material slab, and a bottom silver substrate. To enhance microcavity efficiency and performance, we compare the reflection coefficients of silver half-spaces and a DBR of various number of alternating layer pairs used as a substrate reflector.

$$\alpha_H d_H = \alpha_L d_L = \frac{\lambda_0}{4}, \tag{8}$$

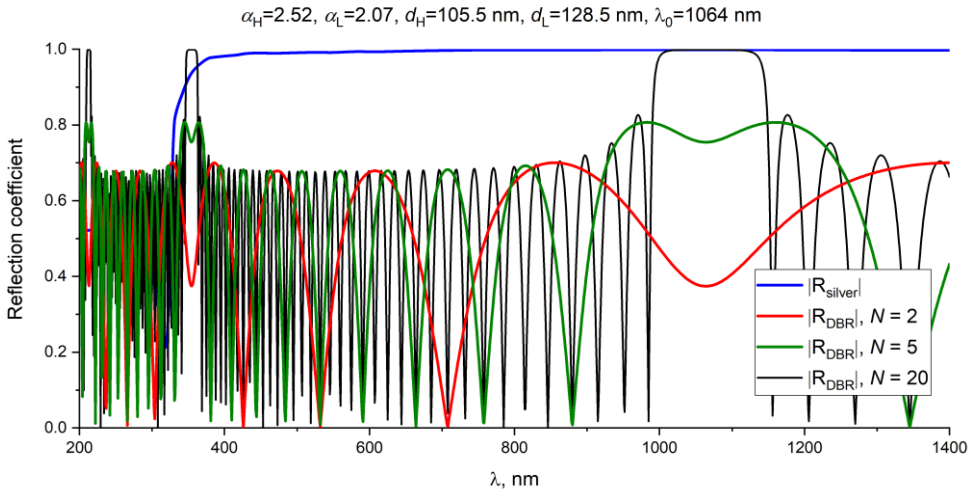

Fig. 2. The absolute values of reflection coefficient of several cavity substrates: silver halfspace and DBR with N = 2, 5, and 20 layer pairs

Their reflection coefficients comparison in the visible and near infra-red ranges is shown in Fig. 2. The DBR is designed for the wavelength of around 1064 nm. The results are presented for 2, 5, and 20 pairs of dielectric layers (e.g. SiO and TiO_2) with α_L = 2.07 and α_H = 2.52, each layer thickness is a quarter of that wavelength, as suggest (8), in the corresponding material, so that w_L = 128.5 nm and w_H = 105.5 nm.

A 2-pair and 5-pair DBR are clearly improper for good reflection, as they yield a reflection coefficient of only under 0.8. As one can see, the widest 20-pairs DBR band gap is located between 1000 and 1150 nm, which corresponds to a high-reflection band. The other much narrower band gaps can be seen between 340 and 360 nm and around 220 nm. The reflection coefficient of silver halfspace at 1064 nm give $|R|_{\text{Ag}}$ = 0.998. In contrast 20-pair DBR has reflection around $|R|_{\text{DBR}}$ = 0.9999 at this wavelength, making it more effective for providing optical feedback.

For the selected configuration, we compute the locations of the LEP eigenvalues and display them on colour maps of the function $|\Phi(\lambda,\gamma)|$, for the $\alpha_c = 1.81$, w_c = 230 nm cavity with 10-nm and 100-nm thick silver films for DBR substrate of 2 and 20 pairs of alternating TiO_2 and SiO layers (Fig. 3).

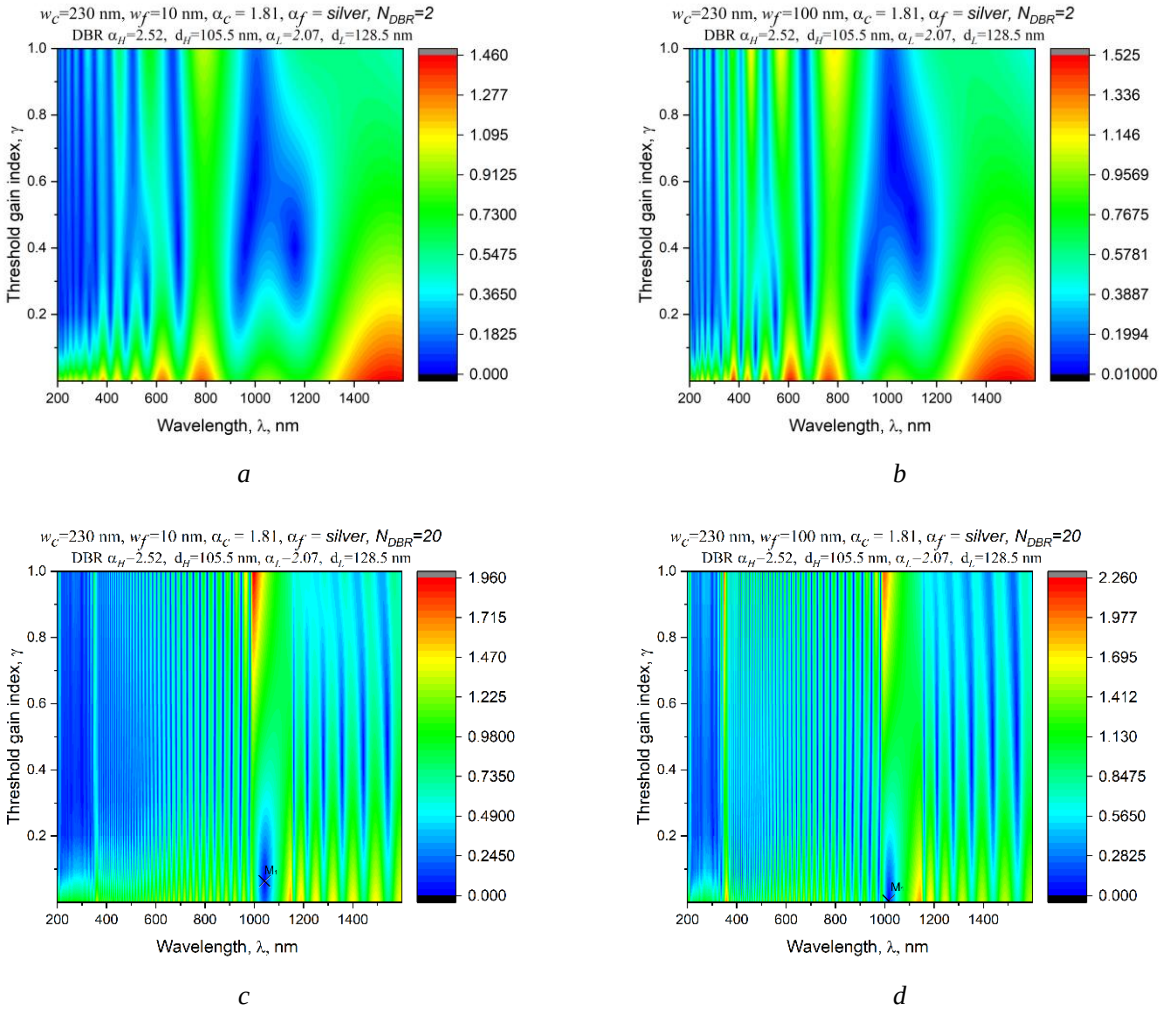

Fig. 3. Colour maps of the absolute value of (4) on the plane of threshold gain index and wavelength for the 2 (*a*), (*b*) and 20 (*c*), (*d*) pairs DBR substrate active microcavity of refractive index α_c = 1.81 with 10-nm (*a*), (*c*) and 230-nm (*b*), (*d*) bulk silver films.

As well visible in Fig. 3, *a*, *b*, there are prominent blue spots, represent the lasing eigenvalue modes. Among them, some exhibit significantly lower threshold gain index values than the others. Here, the influence of the DBR is less pronounced; however, as the thickness of the silver metal

film increases, the threshold value of the mode decreases noticeably. This effect is well visible for M_1, marked with cross, for DBR with 20 pair of alternating layers in Fig. 3, c, *d*. In contrast to our previous model of the same cavity embedded in a silver or even gold environment in [25], the addition of large quantity of DBR layers as substrate in the current configuration shows new modes within the visible and near-infrared ranges. These modes appear in a form of many blue dips on the colour maps. Moreover, increasing the number of layer pairs, *N*, results in a greater number of emerging modes. That means they can be identified as "parasitic" modes of every DBR sub-cavity.

Fig. 3, *c* illustrates that mode M_1, with a wavelength around 1050 nm, lies within the primary band gap, and it has a lower γ, than for less pair quantity DBR configuration. This effect arises because, within its band gaps, the DBR effectively suppresses field leakage into the free halfspace. As a result, the emission threshold is reduced for cavity modes whose frequencies fall within the band gaps. In contrast, all other "parasitic" modes exhibit higher thresholds compared to the "matched" mode mentioned earlier – in the case of mode M_1, which has the lowest threshold. This behaviour can be attributed to the weak overlap between the electric fields of the DBR modes and the active region [18]. The impact of thicker silver film superstrate is similar to 2-pair DBR and shown in Fig. 2, *d*.

Further, we present the first mode M_1 trajectories for the considered microcavity with 20-pair DBR substrate and silver superstrate film under the variation of two thicknesses w_f and w_c in Fig. 4, *a*, *b*, respectively. The DBR's photonic band gap centred around 1064 nm, for example for Nd:YAG active crystal, indicated by the dashed line in the figures. As shown, careful adjustment of either the silver film (Fig. 4, *a*) or the active layer (Fig. 4, *b*) thickness allows more precise tuning of the target emission wavelength, which is of particular importance in lasers.

Note that the threshold gain index value for variation of silver film thickness linearly decreases, while, for variation of active layer thickness stops dropping dramatically from some value of w_c.

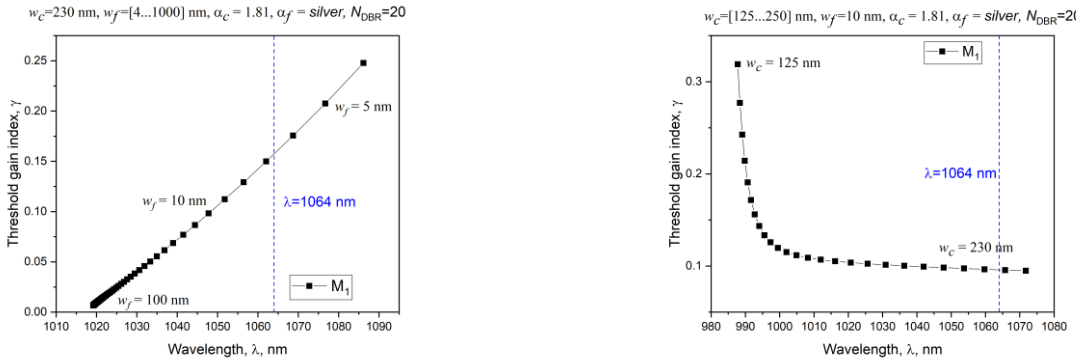

a *b*

Fig. 4. Trajectories of the modes M_1 of the active microcavity covered with silver film and lying on 20-pairs DBR under the variation of the silver film thickness w_f from 4 to 1000 nm (*a*) and active layer thickness w_c from 125 to 250 nm (*b*)

Conclusion

The 1-D mathematical model of layered microlaser threshold condition analysis has been presented. The study has examined how variations in the active layer and silver film thickness, along with the structure of the DBR, specifically the number of alternating dielectric layers, affect the emission wavelength and threshold gain index of the operating modes. For parametric analysis of the lasing eigenvalues the Lasing Eigenvalue Problem approach and Transfer Matrix Method have been used. The numerical results have demonstrated that both the emission frequency and the threshold gain index can be effectively tuned by adjusting the thickness of the silver superstrate film and the number of DBR layer pairs. Moreover, the influence of the DBR extends beyond the formation of photonic band gaps; it also leads to the emergence of numerous "parasitic" modes, which appear to originate from the DBR layers acting as unintended resonant cavities. The number of

these modes scales with the number of alternating high- and low-refractive-index layers in the DBR. Compared to the primary operating mode, these modes have exhibited considerably higher threshold gain values due to their radiation losses are suppressed by the DBR structure. Consequently, the properties of the band gap could be used to isolate the working mode by selecting the parameters of the DBR, thereby eliminating the influence of parasitic modes.

References:

1. Wang X., et al. Beam Scanning and Capture of Micro Laser Communication Terminal Based on MEMS Micromirrors // Micromachines. 2017. Vol. 14, №7. P.1917. doi: 10.3390/mi14071317

2. Feng J., et al. Random Organic Nanolaser Arrays for Cryptographic Primitives // Advanced Materials. 2019. Vol. 31, № 36. art.no. 1807880. doi: 10.1002/adma.201807880

3. Tsunekane M., Taira T. Long Time Operation of Composite Ceramic Nd:YAG/Cr:YAG Micro-chip Lasers for Ignition // Laser Ignition Conference. 2015. p. T4A.3. doi: 10.1364/lic.2015.t4a.3

4. Xu J., McCulloch D., Charlton M. D. B. Modeling full PCSELs and VCSELs using modified rigorous coupled-wave analysis // Optics Express. 2024. Vol. 32, № 13. P. 22169. doi: 10.1364/oe.522484

5. Moon S. et al. High Performance Thin Film VCSELs Integrated with a Copper Plated Heatsink // Advanced Materials Interfaces. 2023. Vol. 10, № 18. art.no. 2300191. doi: 10.1002/admi.202300191

6. Yu H., Wang L., Xu J., Chiang P. Y. A dToF Ranging Sensor with Accurate Photon Detector Measurements for LiDAR Applications // Sensors. 2023. Vol. 23, № 6. P. 3011. doi: 10.3390/s23063011

7. De Zoysa M., et al. Non-mechanical three-dimensional LiDAR system based on flash and beam-scanning dually modulated photonic crystal lasers // Optica. 2023. Vol. 10, № 2. P. 264. doi: 10.1364/optica.472327

8. Chen Z., Dong G., Barillaro G., Qiu J., Yang Z. Emerging and perspectives in microlasers based on rare-earth ions activated micro-/nanomaterials // Progress in Materials Science. 2021. Vol. 121. P. 100814. doi: 10.1016/j.pmatsci.2021.100814

9. Lin J., et al. Low-threshold whispering-gallery-mode microlasers fabricated in a Nd:glass substrate by three-dimensional femtosecond laser micromachining // Optics Letters. 2013. Vol. 38, № 9. P. 1458. doi: 10.1364/ol.38.001458

10. Lin H., et al. Diode-pumped tape casting planar waveguide YAG/Nd:YAG/YAG ceramic laser // Optics Express. 2015. Vol. 23, № 6. P. 8104. doi: 10.1364/oe.23.008104

11. Frigenti G., et al. Rare earth-doped glass whispering gallery mode micro-lasers // The European Physical Journal Plus. 2023. Vol. 138, № 8. art. no. 679. doi: 10.1140/epjp/s13360-023-04275-9

12. Li H., Wang Z., Wang L., Tan Y., Chen F. Optically pumped Milliwatt Whispering-Gallery microcavity laser // Light: Science & Applications. 2023. Vol. 12, № 1. art.no. 223. doi: 10.1038/s41377-023-01264-6

13. Tsutsumi N., Ishibashi T. Organic dye lasers with distributed Bragg reflector grating and distributed feedback resonator // Optics Express. 2009. Vol. 17, № 24. P. 21698. doi: 10.1364/oe.17.021698

14. Arshavsky-Graham S., Massad-Ivanir N., Segal E., Weiss S. Porous Silicon-Based Photonic Biosensors: Current Status and Emerging Applications // Analytical Chemistry. 2018. Vol. 91, № 1. P. 441–467. doi: 10.1021/acs.analchem.8b05028

15. Lu Q., Chen D., Wu G., Peng B., Xu J. A hybrid plasmonic microresonator with high quality factor and small mode volume // Journal of Optics. 2012. Vol. 14, № 12. P. 125503. doi: 10.1088/2040-8978/14/12/125503

16. Yevtushenko D. O., Dukhopelnykov S. V. Visible light from modulated electron beam moving between twin circular silver nanowires forming plasmonic photonic molecule // Journal of Optics. 2020. Vol. 22, № 2. P. 025002. doi: 10.1088/2040-8986/ab65d8

17. Lu Y.-J., et al. Plasmonic Nanolaser Using Epitaxially Grown Silver Film// Conference on Lasers and Electro-Optics. 2012. P. CTh5C.7. doi: 10.1364/cleo_si.2012.cth5c.7

18. Smotrova E. I., Byelobrov V. O., Benson T. M., Ctyroky J., Sauleau R., Nosich A. I. Optical Theorem Helps Understand Thresholds of Lasing in Microcavities With Active Regions // IEEE Journal of Quantum Electronics. 2011. Vol. 47, № 1. P. 20–30. doi: 10.1109/jqe.2010.2055836

19. Byelobrov V. O., Nosich A. I. Mathematical analysis of the lasing eigenvalue problem for the optical modes in a layered dielectric cavity with a quantum well and distributed Bragg reflectors // Optical and Quantum Electronics. 2007. Vol. 39, № 10–11. P. 927–937. doi: 10.1007/s11082-007-9159-4

20. Shapoval O. V., Kobayashi K., Nosich A. I. Electromagnetic Engineering of a Single-Mode Nanolaser on a Metal Plasmonic Strip Placed into a Circular Quantum Wire // IEEE Journal of Selected Topics in Quantum Electronics. 2017. Vol. 23, № 6. P. 1–9. doi: 10.1109/jstqe.2017.2718658

21. Natarov D. M., Benson T. M., Nosich A. I. Electromagnetic analysis of the lasing thresholds of hybrid plasmon modes of a silver tube nanolaser with active core and active shell // Beilstein Journal of Nanotechnology. 2019. Vol. 10. P. 294–304. doi: 10.3762/bjnano.10.28

22. Herasymova D. O., Dukhopelnykov S. V., Natarov D. M., Zinenko T. L., Lucido M., Nosich A. I. Threshold conditions for transversal modes of tunable plasmonic nanolasers shaped as single and twin graphene-covered circular quantum wires // Nanotechnology. 2022. Vol. 33, № 49. P. 495001. doi: 10.1088/1361-6528/ac8e0c

23. Kaliberda M. E., Pogarsky S. A., Kostenko O. V., Nosych O. I., Zinenko T. L. Circular quantum wire symmetrically loaded with a graphene strip as the plasmonic micro/nano laser: threshold conditions analysis // Optics Express. 2024. Vol. 32, № 7. P. 12213. doi: 10.1364/oe.514643

24. Herasymov S.S., Hnatenko O.S., et al. Threshold Conditions for 1-D Model of Laser with Partial Active Region // Journal of Nano- and Electronic Physics. 2024. Vol. 16, № 4. P. 040331-040338. doi: 10.21272/jnep.16(4).04033

25. Herasymov S.S., Hnatenko O.S. Threshold Conditions for 1-D Model of Laser Cavity Covered with Noble Metal Film // Proc. IEEE 5th KhPI Week on Advanced Technology (KhPIWeek 2024). 2024. P. 1–4.

26. Johnson, P. B., Christy, R. W. Optical constants of the noble metals // Physical Review B. 1972. Vol. 6. P. 4370–4379.

Received 05.07.2025

Information about the authors:

Oleksandr S. Hnatenko – Ph.D., Head of Department of Physical Fundamentals of Electronic Engineering, Kharkiv National University of Radio Electronics, Ukraine, email: oleksandr.hnatenko@nure.ua; ORCID: https://orcid.org/0000-0001-7722-0923

Serhii S. Herasymov – student, Department of Physical Fundamentals of Electronic Engineering, Kharkiv National University of Radio Electronics, Ukraine, email: serhii.herasymov@nure.ua; ORCID: https://orcid.org/0009-0005-1127-7544